Influence of thermally radiative dissipative magnetohydrodynamics movement of nanofluid over an exponentially elongating sheet

Shaik Mohammed Ibrahim

Department of Mathematics, Koneru Lakshmaiah Education Foundation, Vaddeswaram, Guntur, Andhra Pradesh- 522302, India

Email ID: ibrahim@kluniversity.in

Abstract:

In the present chapter, I focused a numerical examination of the possessions dissipation of viscous on the thermally radiative of a magneto-hydrodynamics (MHD) movement of an in-compressible nano-fluid caused by an exponentially stretched sheet subject to heat and mass (HMT) fluxes at the boundary layer. To numerically solve the governing PDEs, we first use self-similarity transformation to convert them into a set of ODEs, which we then solve using the shooting technique and a fourth order Runge-Kutta method. The effects of a wide variety of limitations are demonstrated with respect to the non-dimensional flow, temperature, percentage of nano-particle capacity, and local Nusselt and Sherwood number. Calculated and analysed are the friction factor coefficient values, as well as the regional Nusselt (rate of heat transfer) and Sherwood (rate of mass transfer) numbers. Graphs have been employed to make a detailed comparative analysis at deviatedvalues of governing parameters. This article will help to fill that gap by offering a thorough analysis of the exponentially stretched sheet with HMT of nanofluid.

Keywords: *Thermal Emission; MHD; Nanofluid; heat and mass fluxes; Viscous Dissipation.*

1. Introduction

Fluid flow caused by stretched sheets has become an extremely interesting topic over the past decade due to its many industrial uses. Several scientists have examined the issue of boundary layer flow and heat transmission over a linearly stretched sheet. In reality, linearly stretched sheet may not occur always. The pioneering work in investigating the Newtonian flow

induced by a stretched sheet was conducted by Crane [1]. Building upon Crane's work, subsequent researchers have expanded the understanding of this phenomenon by considering the influence of mass transport in deviated contexts. Examples include the contributions of authors [2-4]. Exploring the realm of heat conduction, Nadeem et al. [5] delved into the behavior of a H_2O-based nanofluid using an exponentially stretched sheet. Additionally, Bhattacharyya [6] examined the conduction of both heat and mass across a rapidly contracting sheet within the edge layer. Mukhopadhyay and colleagues [7] conducted an exploration into the transport of high-temperature flow through a permeable exponentially stretched sheet, taking into account thermal radiation. Sajid and Hayat [8] delved into the effects of heat generation on the boundary layer flow caused by an exponentially stretched sheet. Investigating scenarios involving velocity slip and a magnetic field, Zhang et al. [9] centered their research on the heat transport within a power-law nanofluid thin film induced by a stretched sheet. Majeed et al. [10] provided a study of the boundary layer flow of a ferromagnetic fluid across a stretched surface. Using an unsteady stretched sheet, Pal and Saha [11] examined HMT within a thin liquid film, considering the influence of nonlinear thermal emission. Stretched surfaces were integrated into Weidman's investigation [12], which aimed to establish a incorporated design for stagnation point flows.

Magnetohydrodynamics (MHD) is the study of how electrically conducting fluids interact with magnetic fields. This field of study has many important applications, including: Cooling nuclear reactors by liquid sodium: MHD can be used to generate a strong magnetic field that can guide the flow of liquid sodium through a nuclear reactor. This helps to remove heat from the reactor core and prevent it from overheating. Induction flow meters: These devices measure the flow rate of a fluid by measuring the potential difference that is created when the fluid flows through a magnetic field. "In recent decades, Magnetohydrodynamics (MHD) boundary layer flow over a continuously stretching sheet has emerged as a topic of significant interest. This heightened attention can be attributed to its wide-ranging applications across deviated industrial sectors. Notably, this phenomenon finds utility in processes like aerodynamic extrusion of plastic sheets, liquid film formation, hot rolling of metals, wire drawing, glass fiber and paper production, plastic film extrusion, metal and polymer extrusion, and metal spinning, underscoring its importance in diverse manufacturing contexts."

In progressive metallurgic & metal-working activities, the utilization of magnetohydrodynamic (MHD) flow of electrically conductive fluids over stretched sheets has been creatively adopted. Industrial polymer operations frequently involve the continuous extraction of strips and filaments from a moving fluid for cooling purposes. The configuration of the boundary layer adjacent to the stretched sheet holds significant influence over the cooling rate, consequently exerting a profound impact on the final product. Mukhopadhyay and colleagues [13] explored the magnetohydrodynamics flow of a Casson fluid triggered by an exponentially stretched sheet with heat emission. Examining the effects of magnetohydrodynamics, coupled with second-order slip flow and homogeneous-heterogeneous reactions, Hayat et al.[14] conducted a study on bidirectional nanofluid flow. Lin et al. [15] focused their investigation on a stretched surface with internal heat generation, studying the flow and (heat transfer) HT of an unstable MHD nanofluids of pseudo-plastic within a predictable tinny film. To assess the effect of thermal radiation on the flow and heat transfer of magnetohydrodynamic nanofluids, Sheikholeslami et al. [16] adopted a two-phase model. In the context of an MHD Falkner-Skan nanofluid stream, Farooq et al. [17] showcased the application of the HAM-built Mathematica tool BVP h 2.0. Exploring the consequences of thermal emission in a 3D Jeffrey nanofluid stream characterized by inner heat generation and a magnetic field, Shehzad and colleagues [18] carried out an analytical investigation.

The significance of radiation in processes conducted under extremely high temperatures cannot be overstated. Radiative effects find application in turbines of gas, missiles, airplanes, spacecraft, and nuclear power plants. Moradi et al. [19] examined the interplay of emission in a thermally convective viscous liquid flow across an inclined surface. Employing a two-phase model, Sheikholeslami and their research team, in their work referenced as [20], explored the implications of radiation within the context of a viscous nanofluid flow. Their study involved examining the behavior of a laminar flow comprising an Oldroyd-B liquid infused with nanoparticles while considering the influence of radiation. Hayat et al. [21] conducted their study. Ashraf et al. [22] conducted research on a radiative three-dimensional Maxwell fluid flow involving thermophoresis and convective conditions. Hayat and colleagues [23] took a close look at how heat radiation can shape the flow of a Powell-Eyring nanofluid over a stretched sheet.

Several studies have been conducted to explore the impact of deviated factors on fluid flow and heat transfer in deviatedcontexts. Bidin and Nazar [24] focused on examining the

influence of thermal emission on a continuously laminar two-dimensional boundary layer flow over an exponentially stretched sheet. Hady et al. [25] investigated the effects of emission in a viscous nanofluid flow over a nonlinearly stretched sheet, utilizing the fourth-order Runge-Kutta method. Hayat and their colleagues [26] delved into the interplay of Joule heating and thermophoresis in a stretched stream, modeling it with the Maxwell equations under convection conditions. Mustafa et al. [27] addressed the Sakiadis flow of a Maxwell fluid while considering convective boundary conditions. In their research, Hayat et al. [28] examined the stagnation point flow of a Maxwell fluid in the presence of both thermal emission and convection. Additionally, Hayat et al. [29] investigated the effects of an inclined magnetic field on heat generation in a nanofluid flow, considering non-linear thermal emission. Finally, Khan and their co-authors [30] conducted a study on the nonlinear radiative flow of a three-dimensional Burgers nanofluid, incorporating a novel concept related to mass flux.

Motivated by the aforementioned fruitful studies and the significance of HMT in nanofluid flow transport in deviated applications of magnetic field parameters, we are currently attempting to present a study that investigates a novel theoretical approach to deliberate the temperature- and concentration dependent electrical conductivity effects on the transport of a Newtonian nanofluid past an exponentially stretched sheet with considering several physical aspects such as viscous dissipation, radiative and porous medium as well as thermal and mass convection. This investigation is pertinent to a scenario involving an exponentially stretched sheet subjected to heat and mass flux conditions. Similarity transformations are like a magic spell that can turn complex PDEs into simple ODEs. Once the PDEs have been transformed, they can be solved using the Shooting technique, which is like a guided tour through the solution space. Findings are well discussed by usage of both graphical illustrations and tabular representation. The forthcoming sections of this study are organized into specific categories. Section 2 focuses on the mathematical aspects of modeling Newtonian fluid behavior in two-dimensional flows. This section also delves into the dynamics of nanofluid motion patterns, particularly examining the characteristics of Double Diffusion convection. The procedure of numerical method was explained in Section.3. The conceptual framework is highlighted in Section 4 along with depicts a graphically reasonable interpretation of the acquired data; and Section 5 summarizes the problem's final conclusions.

The reviewed literature reveals that no single study has shown how to analyze the numerical treatment for creeping flow through an exponentially stretched sheet with a magnetic flow of nanofluid model saturated in a porous medium with mixed efficiency of diffusion-thermo impacts and thermo diffusion while considering variable electrical conductivity, our work will help to fill that gap. Moreover, the present research is relevant to electromagnetic biomaterials micro-scale pumps that mimic real working fluids and use stretched sheet. Due to their ability to circumvent contamination issues, require minimal maintenance, and exhibit superior durability and efficiency, these pumps possess significant promise for the development of bio-inspired, portable intravenous drip systems, enhancing medical procedures in the 21st century.

2. Mathematical Formulation

An exponentially stretched sheet is employed as a model for a 2D hydromagnetic flow of an incompressible fluid. The analysis of heat and mass transport encompasses factors such as thermal radiation, viscous dissipation, heat generation, and chemical reactions. Additionally, a non-uniform magnetic field denoted as B(x) = B0exp(x/2l) is introduced in the y-direction. In scenarios involving low magnetic Reynolds numbers, the contribution of the induced magnetic field is neglected. Boundary conditions involving heat and mass flux are applied at the sheet's surface. The foundational principles of motion are represented by the following equations:

(i) Continuousness Equation:

$$\frac{\partial u}{\partial x}+\frac{\partial u}{\partial y}=0 \tag{1}$$

(ii) Motion Equations:

$$u\frac{\partial u}{\partial x}+v\frac{\partial u}{\partial y}=\nu\frac{\partial^2 u}{\partial y^2}-\frac{\sigma B_0^2}{\rho}u-\frac{\nu}{K^*}u \tag{2}$$

(iii) Energy:

$$u\frac{\partial T}{\partial x}+v\frac{\partial T}{\partial y}=\alpha\frac{\partial^2 T}{\partial y^2}+\frac{(\rho c)_p}{(\rho c)_f}\left[D_B\frac{\partial C}{\partial y}\frac{\partial T}{\partial y}+\frac{D_T}{T_\infty}\left(\frac{\partial T}{\partial y}\right)^2\right] -\frac{1}{\rho c_p}\frac{\partial q_r}{\partial y}+\frac{\mu}{\rho c_p}\left(\frac{\partial u}{\partial y}\right)^2 \tag{3}$$

(iv) Nanoparticle volume fraction:

$$u\frac{\partial N}{\partial x}+v\frac{\partial N}{\partial y}=D_B\frac{\partial^2 N}{\partial y^2}+\frac{D_T}{T_\infty}\frac{\partial^2 T}{\partial y^2} \tag{4}$$

The associated boundary conditions are defined as

$$u=U_w(x)=\mathrm{U}_0\exp\left(\frac{x}{l}\right),\ v=-V(x),$$
$$\frac{\partial T}{\partial y}=-\frac{q_w(x)}{\alpha},\ \frac{\partial N}{\partial y}=-\frac{q_{np}(x)}{D_B},\ \ at\ y=0 \tag{5a}$$

$$u\to 0,\ T\to T_\infty,\ N\to N_\infty,\ \text{as}\ y\to\infty \tag{5b}$$

Where the point *u* & *v* denote the flow mechanism in the *x* & *y* information respectively, ν a kinematic viscosity, $\alpha=\frac{k}{\rho c_p}$ a thermal diffusivity, k a fluid density, ρ a thermal conductivity, c_p a specific heat, T noted as temperature of fluid, T_∞ denotes ambient temperature, N a fluid concentration, C_∞ a ambient concentration, $\alpha=k/\rho c_p$ a thermal diffusivity, k a thermal conductivity, c_p a specific heat, $q_r=\frac{16\sigma^* T_\infty^3}{3k^*}\frac{\partial T}{\partial Y}$ represents radiative heat flux, k^* a mean absorption coefficient, σ^* indicates Stefan-Boltzmann constant, $(\rho c)_p$ noted for prominence heat capacity of nanoparticles, $(\rho c)_f$ heat capacity of the base fluid. N is nanoparticle volume, D a mass diffusion $U_w(x)=\mathrm{U}_0\exp(x/l)$ is a stretched stream of sheet, U_0 a reference stream, l a reference length, $q_w(x)=q_{w0}\,\mathrm{T}_0\sqrt{U_0/2vl}\exp(x/l)$ the variable heat flux, $q_{np}(x)=q_{np0}C_0\sqrt{U_0/2vl}\exp(x/l)$ a variable surface nanoparticle flux, U_0, T_0, q_{w0}, q_{np0}, N_0, are the reference stream, temperature and heat flux, surface nanoparticle flux, nanoparticle capacityfraction respectively, $V(x)=V_0\exp(x/l)$ a special type of stream at the wall is considered (Bhattacharyya [30]) where V_0 is a constant. Here $V(x)>0$ is the stream of suction and $V(x)<0$ is the stream of injection.

Applying similarity transformations as follows

$$\eta = y\left(\frac{U_0}{2\nu x}\right)^{1/2}\exp\left(\frac{x}{l}\right),\ \psi = \left(2\nu U_0 x\right)^{1/2} f(\eta)\exp\left(\frac{x}{l}\right),$$

$$u = U_0 f'(\eta)\exp\left(\frac{x}{l}\right),\ v = -\sqrt{\frac{\nu U_0}{2l}}\exp\left(\frac{x}{l}\right)\left[f(\eta) - \eta f'(\eta)\right], \tag{6}$$

$$T = T_\infty + \frac{q_{w0}}{\alpha}T_0\exp\left(\frac{x}{l}\right)\theta(\eta), C = C_\infty + \frac{q_{np0}}{\alpha}C_0\exp\left(\frac{x}{l}\right)\phi(\eta)$$

If the dimensional stream function $\psi(x, y)$ then $u = \frac{\partial\psi}{\partial y}$ and $u = -\frac{\partial\psi}{\partial x}$.

The continuity equation is inherently satisfied, and upon implementing a similarity transformation, equations (2), (3), and (4) evolve into

$$f''' + ff'' - 2f'^2 - (Ha + K)f' = 0 \tag{7}$$

$$\left(1 + \frac{4}{3}R\right)\theta'' + \Pr\left(f\theta' + f'\theta + N_b\theta'\phi' + N_t\theta'^2\right) + \Pr Ec\left(f''\right)^2 = 0 \tag{8}$$

$$\phi'' + Le(f\phi' - f'\phi) + \frac{N_t}{N_b}\theta'' = 0 \tag{9}$$

At this point primes mean differentiation with respect to η, $Ha = \frac{\sigma B_0^2(x)l}{\rho U_w(x)}$ is a Hartmann numbers, $\Pr = \frac{\nu}{\alpha}$ is a Prandtl numbers, $R = \frac{4\sigma^* T_\infty^3}{kk^*}$ is a emission constraint and $Le = \frac{\nu}{D_B}$ is a Lewis numbers, $N_b = \frac{(\rho c)_p q_{np0}}{(\rho c)_f \nu}N_0$ is a Brownian motion constraint, $Ec = \frac{U_0^2}{T_0\rho c_p}$ is a Eckert numbers, and $N_t = \frac{D_T}{T_\infty}\frac{(\rho c)_p q_{w0}}{(\rho c)_f \alpha\nu}T_0$ is a thermophoresis constraint, respectively.

The converted frontier conditions (5a) and (5b) are given by

$$\begin{aligned} &f = S,\ f' = -1, \theta = -1, \phi = -1 \quad at\ \eta = 0 \\ &f' = 0,\ \theta = 0,\ \phi = 0 \qquad\qquad as\ \eta \to \infty \end{aligned} \tag{10}$$

Wherever $S = \frac{-v_0}{\sqrt{\nu c/2l}}$ is injection/suction restraint. Here the constraint is positive S >0 (v_0 <0) for mass suction and negative S <0 (v_0 >0) for mass injection.

Furthermore, researchers have taken a keen interest in the intriguing parameters of the skin friction coefficient (Cf), the local Sherwood number (Shx), and the local Nusselt number (Nux). These parameters serve as indicators of the shear stress on the surface and the mass and heat transfer characteristics related to fluid flow

$$\sqrt{2C_f \operatorname{Re}_x} = f''(0),\ C_f = \frac{u}{U_w \exp(x/l)}\left(\frac{du}{dy}\right)_{y=0}, \tag{11}$$

As of the temperature distribution, we be able to examine the heat transport rate, which is expressed as:

$$\frac{Nu_x}{\sqrt{\operatorname{Re}_x}} = -\sqrt{\frac{x}{2l}}\left(1+\frac{4}{3}R\right)\theta'(0),\ Nu_x = -\frac{x}{(T_w - T_\infty)}\left(\frac{\partial T}{\partial y}\right)_{y=0} \tag{12}$$

As of the concentration retrieve, we will be able to illustrate the rate of mass transportation which is specified by

$$\frac{Sh_x}{\sqrt{\operatorname{Re}_x}} = -\sqrt{\frac{x}{2l}}\phi'(0),\ Sh_x = -\frac{x}{(C_w - C_\infty)}\left(\frac{\partial C}{\partial y}\right)_{y=0} \tag{13}$$

where $\operatorname{Re}_x = U_0 x/\nu$ the confined Reynolds numbers.

3. Method of solution:

In this section, we employ Mathematica software to derive the non-linear ordinary differential equations (ODEs) represented by equations (7), (8), and (9), which govern the primary partial differential equations (PDEs) given by equations (2), (3), and (4). These equations are transformed using non-dimensional variables to enhance their simplicity, facilitating numerical solutions. The subsequent portion of this section will provide an in-depth explanation of the implementation of the Shooting technique for addressing the current problem A step size of $\Delta\eta = 0.01$ was selected to be satisfactory for a convergence criterion of 10^{-6} in all cases. You can visually obtain the grade results from Figures (1) through (7), and these visualizations will lead to conclusions regarding the stream field and deviated other significant physical parameters of interest

4. Discussion and graphical illustrations:

We have developed a mathematical framework to assess the combined effects of thermal and mass convection, as well as variable electrical conductivity, in a two-dimensional MHD nanofluid flow over an exponentially stretched sheet. In this section, we analyze the flow variables presented in Figures 7-19, which are based on numerical results generated using Mathematica symbolic software. Our investigation focuses on understanding how key electromagnetic and hydrodynamic parameters influence these flow variables. It's essential to keep in mind that all of the derived figures have typical parameter values that are Ha = 1.0, S = 3.0, Le = 1.3, R = 0.1, Pr = 0.71, Ec = 0.1, Nt = 0.8, and Nb = 0.5 are the leading restrictions that are held constant throughout the computations. Suction constraint Hartmann numbers, Eckert numbers Ec, Lewis numbers Le, emission constraint R, thermophoresis numbers Nt, and Brownian motion constraints Nb all have an impact on the stream, temperature, and friction profiles of nano-sized particles. In Figures 1(a) and (b), we see the profiles of the stream, temperature, and nanoparticle capacity friction for deviatedvalues of the suction constraint.
As can be seen in Fig. 1(a), when the suction constraint is raised, the stream profiles go up. when can be seen in Figure 1(b), the temperature decreases when the suction constraint is tightened. Frictional profiles of streams, temperatures, and nanoparticles, as a result of the Hartmann numbers (i.e. the magnetic field constraint Ha), are displayed in Figs. 2(a) and (b). As demonstrated in Fig. 2(a), the stream patterns increase as Hartmann numbers are increased. Physically increasing the magnetic field also increases the Lorentz force. When greater force is used to stop the flow of a fluid, the fluid's velocity increases. As can be seen in Fig. 2(b), as the Hartmann numbers increases, the temperature decreases.

Figure 3(a) and (b) display the effects of the dissipative constraint, Eckert numbers Ec, on the stream and temperature profiles. As the dissipation constraint Ec is raised, the stream and temperature profiles of the stream are shown to expand. Generally speaking, higher viscosities result in higher stream profiles because their enhanced heat conductivity. Figure 4(a)-(b) displays the results of the thermophoresis constraint Nt on the temperature and the nano-particle capacity percent. As shown in Figure 4(a), as the thermophoresis constraint is tightened, both the temperature and nano-particle capacity fraction profiles rise. The thermophoresis constraint Nt is quantified as the ratio of nanoparticle diffusion rate to thermal diffusion rate within the nanofluid.

As the thermophoresis constraint Nt increases, the thermal boundary layer expands due to a greater temperature differential between the sheet and the surrounding fluid. With an increasing Nt, the thermophoresis force intensifies, allowing nanoparticles to migrate from hotter to cooler regions. Consequently, this migration leads to a higher nano-particle concentration. Figure 5(a)-(b) illustrates how the emission constraint R influences the temperature and nano-particle concentration profiles. It's important to remember that a better temperature profile results from a higher R value. This is because the average absorption coefficient drops with increasing R. As can be shown in Fig. 5(b), the fractional capacity of nanoparticles rises with increasing R.

Finally, the impact of the Lewis numbers Le and the Brownian motion constraint Nb on the capacity fraction profiles of nano-particles is depicted in Figs. (6) and (7). when can be seen in Fig. (6), when the Lewis numbers improves, the distribution of the nano-particle capacity fraction narrows. This is because the Brownian diffusion coefficient Nb drops with increasing Le, making it harder for nano-particles to disperse throughout the fluid. Therefore, the capacity percentage of nano-particles decreases as the Lewis statistic Le increases. In addition, the fractional capacity of nanoparticles in the profile falls as the Brownian motion constraint Nb is increased. The thermal boundary layer may become more substantial as a result of this. The physical mechanism by which an increase in Brownian motion decreases the concentration inside the frontier layer is an increase in nano-particle diffusion.

The numerical values for the friction factor term, Nusselt numbers, and Sherwood numbers are presented in Tables 1 and 2. Table 1 indicates that an increase in either the Nusselt numbers (N) or the Eckert numbers (Ec) leads to a reduction in the skin friction coefficient. In contrast, Table 2 reveals that the confined Nusselt and Sherwood numbers decrease with an increase in the significance of the Hartmann number (Ha), while the reverse trend is observed for higher values of the Schmidt number.

Table 1: Statistical values of friction factor term and confined Nusselt numbers for deviated values of *Ec* and *R* when *Ha*=2.0, *Nt*=0.5, *Nb*=0.8, *Pr*=0.73, *R*=0.5, *Ec*=0.5 and *Le* = 1.5.

Constraints(fixed values)	Constraints	$f''(0)$	$\mathrm{Re}_x^{-1/2} Nu_x$

Nt=0.5, Nb = 0.8, S=5.0, Pr=0.73, R=0.5, Le=1.5	R=0.20	1.2205578	0.560558
	0.25	1.216655	0.566655
	0.30	1.197775	0.567775
	Ec=0.0	1.265308	0.559308
	0.3	1.220558	0.560558
	0.5	1.208727	0.568727

Table 2: Statistical values of confined Nusselt numbers and confined Sherwood numbers for discrete values of Ha and S when Ha=2.0, Nt=0.5, Nb=0.8, Pr=0.73, R=0.5, Ec=0.2 and Le = 1.5.

Constraints(fixed values)	Constraints	$\mathrm{Re}_x^{-1/2}\, Nu_x$	$\mathrm{Re}_x^{-1/2}\, Sh_x$
Nt=0.5, Nb = 0.8, S=5.0, Pr=0.73, R=0.5, Le=1.5	Ha=2.0	0.551146	0.394789
	2.5	0.538588	0.387825
	3.0	0.503747	0.367843
	S=0.1	0.515308	0.351434
	0.3	0.523404	0.362578
	0.5	0.540727	0.378441

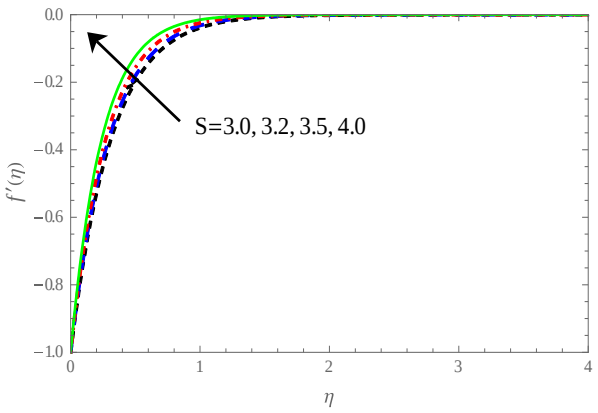

Fig 1(a). Prominence of s on $f'(\eta)$

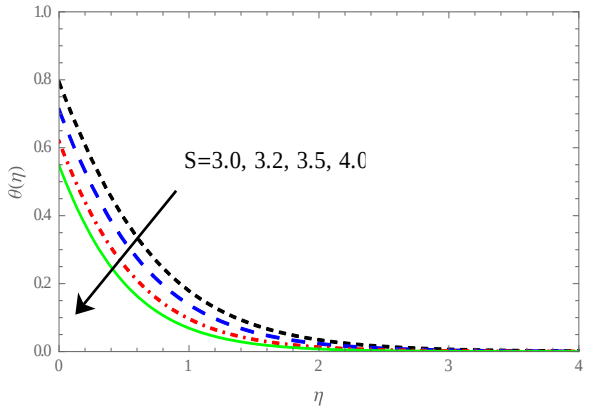

Fig 1(b). Prominence of s on $\theta(\eta)$

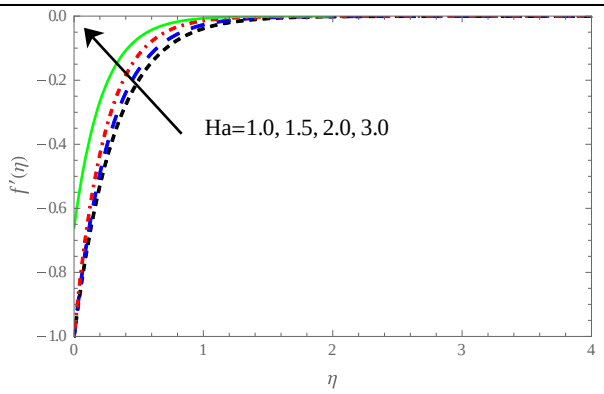

Fig 2(a). Prominence of Ha on $f'(\eta)$

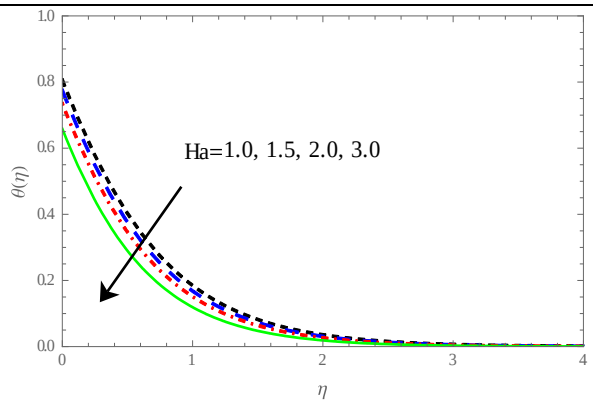

Fig 2(b). Prominence of Ha on $\theta(\eta)$

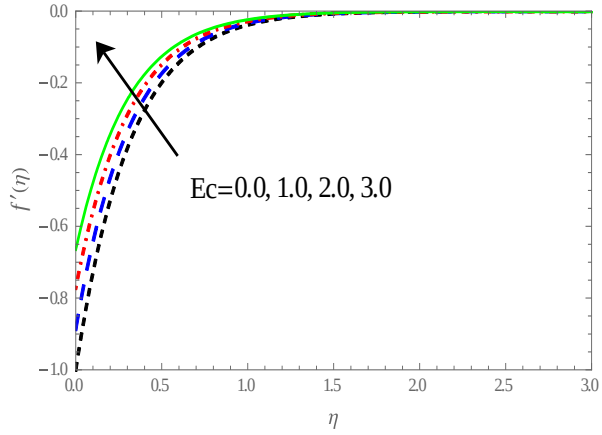

Fig 3(a). Prominence of Ec on $f'(\eta)$

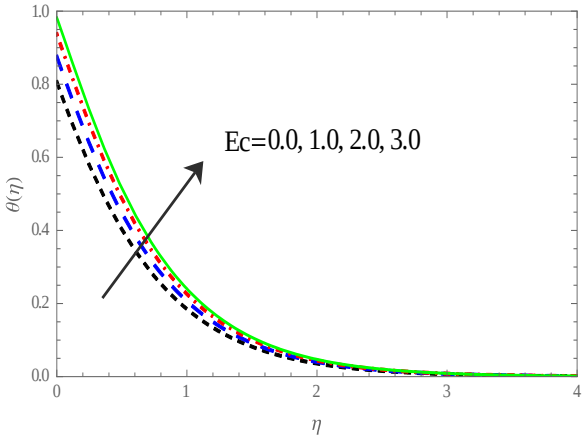

Fig 3(b). Prominence of Ec on $\theta(\eta)$

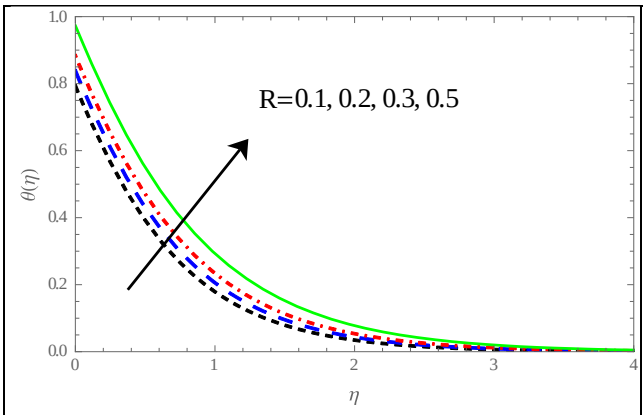

Fig 4(a). Prominence of R on $\theta(\eta)$

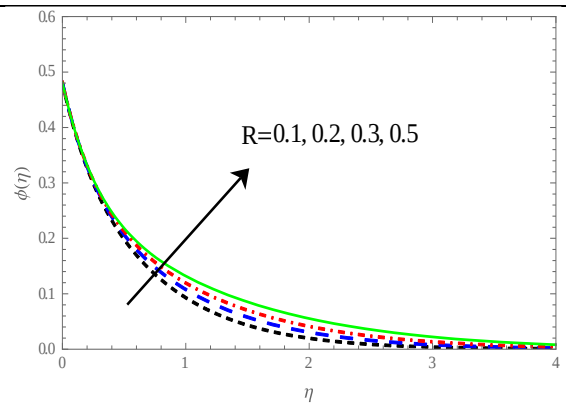

Fig 4(b). Prominence of R on $\phi(\eta)$

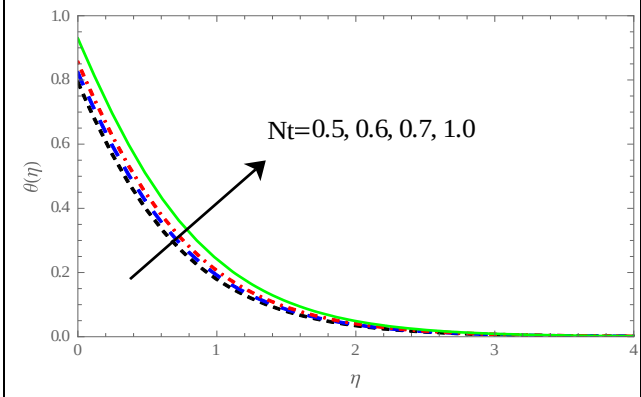

Fig 5(a). Prominence of Ec on $\theta(\eta)$

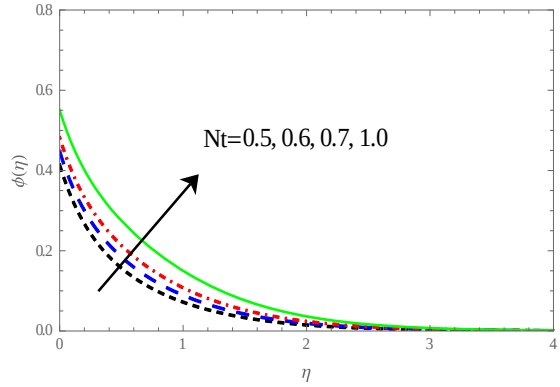

Fig 5(b). Prominence of Ec on $\phi(\eta)$

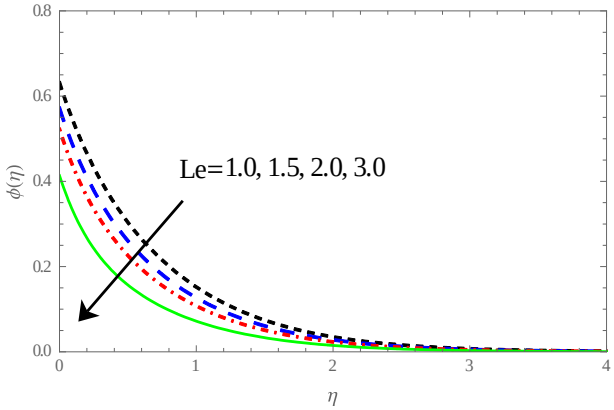

Fig 6. Prominence of Le on $\phi(\eta)$

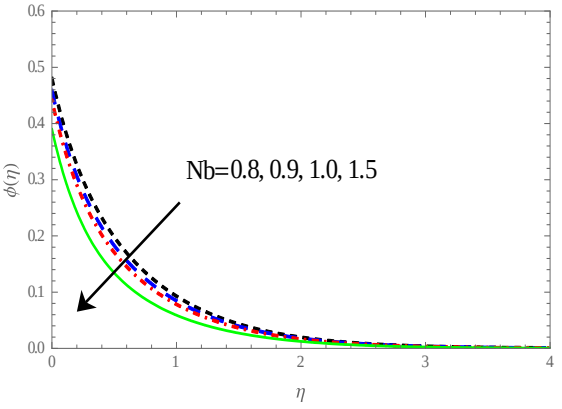

Fig 7. Prominence of Nb on $\phi(\eta)$

Conclusion:

This work outlines a study on heat transport involving an exponentially stretched sheet under conditions of heat and mass flux, while accounting for viscous dissipation. The investigation explores the significance of both thermal emission and Magnetohydrodynamics (MHD) in the

flow of a dissipating viscous nanofluid. The initial system of governing partial differential equations underwent a transformation, resulting in a set of nonlinear coupled ordinary differential equations. These equations were then tackled through a numerical solution approach employing the fourth-order Runge-Kutta shooting method. The research investigates pertinent constraints affecting coefficients associated with friction, skin friction, heat, and mass transfer. These constraints are analyzed in the context of flow behavior, temperature distribution, and nanoparticle concentration, and their implications are graphically depicted and summarized in tables. The primary discoveries of this study are succinctly outlined below:

(i) The suction constraint causes the stream profile and frontier layer thickness to grow. The Hartmann Numbers The Eckert-Harrington numbers Ec.

(ii) Larger suction constraints and Hartmann numbers lead to a lower temperature profile and thinner thermal boundary layer. Ha, but the emission parameter R and Eckert numbers Ec both go down as their values rise.

(iii) When the radiation constraint R and the thermophoresis constraint Nt are both high, the nano-particle capacity fraction rises.

(iv) As the values of R and Ec are constrained, the skin fraction coefficient decreases.

(v) Local Nusselt numbers is increasing function of S, R and Ec.

(vi) Local Sherwood numbers is increasing function of S.

Availability of Data and Material The author can provide access to the study's data upon request.

Conflicts of Interest The author affirms that they do not possess any identifiable conflicting financial interests or personal relationships that might have seemed to exert an influence on the research presented in this chapter.

References:

[1] Crane, L .J.,(1970). Stream past a stretched plate. Zeitschrift für angewandte Mathematik und Physik *ZAMP*, 21(4), 645–647.

[2] Dutta, B. K, Roy P, Gupta, A.S.(1985). Temperature field in flow over a stretched sheet with uniform heat flux. *Int Commun Heat Mass Transport* ,12(1):89–94.

[3] Char, M.I. (1988). Heat transport of a continuous, stretched surface with suction or blowing. *J Math Anal Appl.,* 135(2):568–80.

[4] Gupta ,P.S., and Gupta, A.S., (1977). Warm and mass transport on a stretched sheet with suction or blowing. *Can J Chem Eng,* 55(6):744–746.

[5] Nadeem S, Haq R.U., and Khan Z .H.,(2014). Heat transport analysis of water-based nanofluid over an exponentially stretched sheet. *Alexandria Eng. J.,* 53(1) pp. 219–224.

[6] Bhattacharyya, K., (2011)., Frontierlayer stream and heat transport over an exponentially shrinking sheet, *Chin. Phys. Lett.,* 28(7), 4701.

[7] Mukhopadhya S.,(2013). Slip Prominences on MHD Boundary layer stream over an exponentially stretched sheet with suction/blowing and thermal emission. *Ain Shams Eng J.,* 4(3):485–491.

[8]. Sajid, M., Hayat, T. (2008). Influence of thermal emission on the frontierlayer stream due to an exponentially stretched sheet, *Int. Commun. Heat Mass Transf.* 35, 347–356.

[9] Zhang, Y. Zhang, M, Bai Y.,(2017). Unsteady stream and heat transport of power-law nanofluid thin film over a stretched sheet with variable magnetic field and power-law stream slip Prominence, *J. Taiwan Inst Chem Eng*., 70:104–110.

[10] Majeed A, Zeeshan A, Ellahi R (2016). Unsteady ferromagnetic liquid stream and heat transport analysis over a stretched sheet with the Prominence of dipole and prescribed heat flux, *J Mol Liq* 223:528–533.

[11] Pal D, Saha P (2016). Influence of nonlinear thermal emission and variable viscosity on hydromagnetic warm and masstransport in a thin liquid film over an unsteady stretched surface. *Int J Mech Sci,* Vol. 119:208–216.

[12] Weidman P, Turner M R (2017). Stagnation-point streams with stretched surfaces: a unified formulation and new results. *Eur J Mech B Fluids,* 61, 144–153.

[13] S. Mukhopadhyay, I.C. Moindal, T. Hayat(2014). MHD frontierlayer stream of Casson fluid passing through an exponentially stretched permeable surface with thermal emission, *Chin. Phys*. B, 23 104701-12.

[14] T. Hayat, M. Imtiaz, A(2015). Alsaedi, Impact of magnetohydrodynamics in bidirectional stream of nanofluid subject to second order slip stream and homogeneous–heterogeneous reactions, *J. Magn. Magn. Mater*., 395 294–302.

[15] Y. Lin, L. Zheng, X. Zhang, L. Ma, G. Chen(2015). MHD pseudo-plastic nanofluid unsteady stream and heat transport in a finite thin film over stretched surface with internal heat generation, *Int. J. Heat Mass Transf.*, 84 903–911.

[16] M. Sheikholeslami, D.D. Ganji, M.Y. Javed, R. Ellahi (2015). Prominence of thermal emission on magnetohydrodynamics nanofluid stream and heat transport by means of two phase model, *J. Magn. Magn. Mater.*, 374, 36–43.

[17] U. Farooq, Y.L. Zhao, T. Hayat, A. Alsaedi, S.J. Liao (2015). Application of the HAM-based Mathematica package BVPh 2.0 on MHD Falkner–Skan stream of nanofluid, *Comput. Fluids*, 11 69–75.

[18] S.A. Shehzad, Z. Abdullah, A. Alsaedi, F.M. Abbaasi, T. Hayat (2016). Thermally radiative three-dimensional stream of Jeffrey nanofluid with internal heat generation and magnetic field, *J. Magn. Magn. Mater*., 397, 108–114.

[19] A. Moradi, H. Ahmadikia, T. Hayat, A. Alsaedi(2013). On mixed convection emission interaction about an inclined plate through a permeable medium, *Int. J. Thermal Sci.* 64,129–136.

[20] M. Sheikholeslami, D.D. Ganji, M.Y. Javed, R. Ellahi (2015). Prominence of thermal emission on magnetohydrodynamics nanofluid stream and heat transport by means of two phase model, *J. Mag. Magnetic Materials* 374, 36–43.

[21] Hayat T., T. Hussain, S. Shehzad, A. Alsaedi, A (2015). Stream of Oldroyd-B fluid with nanoparticles and thermal emission, *Appl. Math. Mech.* 36, 69-80.

[22] M. Ashraf, T. Hayat, S. Shehzad, A. Alsaedi(2015) Mixed convection radiative stream of three dimensional Maxwell fluid over an inclined stretched sheet in occurrence of thermophoresis and convective condition, *AIP Adv.* 5, 027134.

[23] Hayat T., N. Gull, M. Farooq, B. Ahmad (2015). Thermal emission Prominence in MHD stream of Powell-Eyring nanofluid induced by a stretched cylinder, *J. Aerospace Eng., ASCE*. 29(1),1943-5525.

[24] Bidin B and Nazar R(2009)., Numerical Solution of the FrontierLayer Stream over an Exponentially Stretched Sheet with Thermal Emission, Eur. J. Sci. Res. **33** (4), 710–717.

[25] Hady F.M, Ibrahim F.S, Abdel-Gaied S.M, Eid M.R (2012) Emission Prominence on viscous stream of a nanofluid and heat transport over a nonlinearly stretched sheet, *Nano Scale Res Lett* 7:299.

[26] Hayat T., M. Waqas, S.A. Shehzad, A. Alsaedi (2014). Prominences of Joule heating and thermophoresis on stretched stream with convective frontierconditions, *Scientia Iranica B* 21, 682–692.

[27] M. Mustafa, J. Khan, T. Hayat, A. Alsaedi(2015). Sakiadis stream of maxwell fluid considering magnetic field and convective frontierconditions, *AIP Adv.*, 5, 027106.

[28] Hayat T., M. Waqas, S. Shehzad, A. Alsaedi(2013). Mixed convection radiative stream of Maxwell fluid near a stagnation point with convective condition, *J. Mech.* 29, 403–409.

[29] Hayat T., S. Qayyum, A. Alsaedi, A. Shafiq(2016). Inclined magnetic field and heat source/sink aspects in stream of nanofluid with nonlinear thermal emission, *Int. J. Heat Mass Transport* 103, 99–107.

[30] Khan, M. Khan, W.A., Alshomrani, A.S. (2016). Non-linear radiative stream of three dimensional Burgers nanofluid with new mass flux Prominence, *Int. J. Heat Mass Transport*, 101, 570–576.